2D Contour Following with an Unmanned Aerial Manipulator: Towards Tactile-Based Aerial Navigation

Salua Hamaza, Ioannis Georgilas, Thomas Richardson

***Abstract*— In this paper we present a force control via energy tanks method for use with an unmanned aerial manipulator for the purposes of 2D contour following. This allows an aerial vehicle to trace out a boundary whilst in continuous contact with a surface through means of an active compliant manipulator. This is a key step towards tactile-based aerial navigation, which can be used to complement more traditional mapping approaches such as visual slam. Our results show that an energy-based approach can be used to apply a constant shear force through the manipulator whilst ensuring the vehicle remains in contact with the surface of interest. Results also show that this is a robust, repeatable approach to aerial tactile interaction and one which has the potential to be used in highly complex, unknown environments.**

I. INTRODUCTION

Robotic manipulation has been at the centre of state-of-the-art of robotics research for over forty years. It has only been relatively recently however that the research community has focused on the development of manipulation capabilities for unmanned aerial vehicles (UAVs). The term *aerial manipulation* has been coined to describe this class of robots that are able to carry out manipulation tasks airborne by means of manipulators mounted on top of the aircraft. Several challenges are faced when interacting with the environment airborne, as the exchange of forces and torques between the end-effector/gripper and the target object affects both the vehicle stability and its dynamic response, often leading to a poor performance or even potential failure.

It was found that compliance is an essential feature for aerial manipulators as it aids stability and improves the overall reliability of the system. Compliance can be introduced in the system as part of the mechanical structure of the manipulator with the use of spring-like elements, or via software through impedance type of controllers. Examples of mechanical compliance can be found in the works of [1], [2] where a lightweight manipulator is equipped with flexible joints and finger module to allows for force-estimation and compensation. In [3] a passively-compliant 1-degree-of-freedom (DoF) manipulator is used for collision absorbance in highly-dynamical scenarios such as impacts. It is shown that the force exerted by aerial system with the compliant element is reduced to a fifth compared to the case where a rigid manipulator is used. *Compliant* control strategies have been developed addressed to the aerial platform only in the form of impedance or adaptive control. These control approaches demonstrate force estimation and motion feedback at the end-effector, improving stable contact during aerial interaction [4]–[7]. In our previous work [8], [9], compliance was introduced in the aerial system in the form of a variable-gain controller for the manipulator, while keeping a standalone flight controller on the aerial platform. Results demonstrated that by adapting the manipulator control gains, the dynamic response of the system as a whole changed and different output forces were generated at the end-effector, allowing us to fine-tune the overall compliant behaviour.

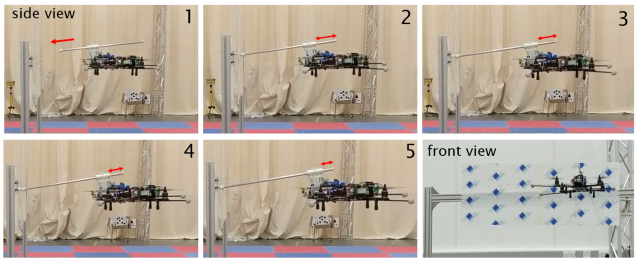

Fig. 1: A sequence of frames captured during flight experiments show a side view of the aerial system whilst exerting a shear force along a 1.25 metres surface by means of a 1-DoF manipulator. The last frame shows a front view of the same experiment.

In this paper we propose a passivity-based force controller via energy tanks tailored for aerial manipulation. This approach will allow for the exertion of a shear force over a surface for a prolonged period of time, maintaining stable and un-interrupted contact with it. The main motivation for this work is to provide the UAV with tactile feedback over the surrounding environment, providing 2D contour following capabilities to aid navigation. Often UAVs are deployed for search and rescue scenarios, for example inside wrecked buildings after an earthquake or other natural calamities. In most cases the aircraft only relies on visual sensing and SLAM for navigation due to occluded GPS signal. Tactile feedback provides the aerial platform with an additional way to safely navigate in poor-lit environments and map such enclosed areas.

The contribution of this work lies in the novel approach to 2D contour following by an aerial vehicle through the use of energy-tank based force control. The control laws have been tailored for a 1-DoF manipulator and integrate the aircraft states resulting in closed-loop control within the manipulator itself. The manipulator also incorporates smart sensing and a high-performance motor controller within a compact design, optimised for force-driven aerial applications. Multiple aerial experiments demonstrate the reliability and robustness of this approach, and offer the potential for more complex contour

This work was supported by the EPSRC Centre for Doctoral Training in Future Autonomous and Robotic Systems (FARSCOPE).

S. Hamaza (s.hamaza@bristol.ac.uk) and T. Richardson are with the Faculty of Engineering, University of Bristol, UK. I. Georgilas is with the Department of Mechanical Engineering, University of Bath, UK.

following tasks.

The outline of this paper presents the modeling of the proposed control laws, followed a section on the manipulation system design, working principle and sensing. In the experiment section, the flight results are presented, in conjunction with the analysis of both the manipulator and aircraft performance. In the last section, a summary of the lessons learned are presented, together with the conclusions and ideas for further work.

A. Related Work

Let us first consider relevant work applied in the field of fixed robots, i.e. industrial robotic arms for assembling purposes. In the works presented in [10], [11] a constrained-based approach that allows to selectively control force, impedance and position has been proposed. The former combines the estimation of geometric uncertainty into the instantaneous task specification and allows for compensation of time-varying coordinates on the end-effector. The latter extends on the to task specification geometry requirements to a guarantee a smoother and more robust indirect force control. Hybrid position/force type of control gained popularity since its formulation three decades ago as it allow to work in force and motion sub-spaces that are complimentary to each other in conjunction with the task specification. Despite the versatility of the hybrid approach, the major drawbacks are associated with the need for an accurate modeling of the contact properties *a-priori* to achieve a good performance, and the lack of robustness during contact-loss [12]. In [13] a unified method combining force and impedance control via energy-tank is presented with a particular focus on contact loss compensation and allows for safe contact and force tracking over 3D surfaces.

Now, moving to force-tracking control approaches designed for aerial manipulators, in [14] a variable-impedance control applied to an aerial platform is proposed, capable of adjusting the impedance of the multi-rotor and regulate the response to time-varying interaction forces. This approach specifically focuses on safe and robust compensation of disturbances exerted by the environment, for example in case a human operator interferes with the manipulator by exerting an external force on it. In [15] forces up to 16 N are applied by an aerial vehicle equipped with a 1-DoF manipulator pitching at high angles against a flat vertical surface. This work control strategy addresses the joint motion over the pitch and yaw angles to guarantee stable contact for prolonged periods of time, however it has the limitation of a static contact point, i.e. it is assumed that the end-effector has enough friction to keep a fixed contact and avoid motion.

In addition to the works cited above, in this paper we propose a force control architecture that includes the concept of energy tanks [16], [17] for stable and prolonged force-tracking and aerial contour following over 2D surfaces. Our proposed approach is the first step towards tactile-based aerial navigation and provides the base ground for further investigation on navigation in un-modeled 3D environments using tactile feedback on an unmanned aerial system.

II. CONTROL

A. Force Control Design

Let us start by introducing force-tracking control designed for a generic n-DoF manipulator using a Proportional-Integral approach. The motor torque τ_m is directly proportional to the Jacobian matrix of the system as follows:

$$\tau_m = J^T(\mathbf{q})\Big[k_p\Big(F(t) - F_d(t)\Big) + k_i \int_0^t \Big(F(t) - F_d(t)\Big)dt\Big] \tag{1}$$

where J^T is the transpose of the Jacobian matrix which only depends on the manipulator's configuration, i.e. the vector of generalised coordinates $\mathbf{q} \in \mathbb{R}^n$. Terms $F(t)$ and $F_d(t)$ are the time-varying force and desired force values respectively, and k_p and k_d the proportional and derivative gains respectively.

Now, let us re-arrange the previous equation for a n-DoF manipultor actuated by brushless DC motors, which present a linear relationship between the input current and output torque. These types of motors are the selected for the proposed manipulation system (described in the next section) as they provide high output torques and the ability to generate higher forces compared to servo or stepper motors of similar size and weight. Therefore, to achieve direct force-tracking on the end-effector the current-to-torque linear relationship is used as follow:

$$\tau_m = J^T(\mathbf{q})\Big[K_T\big[k_p\big(c(t) - c_d(t)\big) + k_i \int_0^t \big(c(t) - c_d(t)\big)dt\big]\Big] \tag{2}$$

where the parameter K_T is the motor's torque-current constant and it is provided by the motor's manufacturer, $c(t)$ and $c_d(t)$ are the input current and desired current respectively.

B. Energy Tank Design

Energy tank-based methods have frequently been used for tasks concerning tele-operated manipulation [18]–[20], but also as an addition to impedance control with variable stiffness [16]. The role of the energy tank is to act as a virtual storage element and minimise the energy dissipation of the controlled system. Such energy represents the *passivity threshold* used by the force controller, and the tank being its reservoir. In essence the tank allows to act upon the impedance of the system by monitoring the amount of energy dissipated during the task and amending the output force accordingly. The tank energy is:

$$T(x_t) = \frac{1}{2}x_t^2 \tag{3}$$

where the variable $x_t(t) \in \mathbb{R}$ is the state associated with the tank, with the condition of $x_t(0) > 0$. Now, the dynamics are given by:

$$\begin{cases} \dot{x}_t = \dfrac{\beta}{x_t}\big(\ \dot{\tilde{x}}^T D_d \dot{\tilde{x}}\ \big) + u_T \\ \tilde{x}(t) = x(t) - x_d(t) \\ u_T = -w(t)^T \dot{\tilde{x}}_t \end{cases} \tag{4}$$

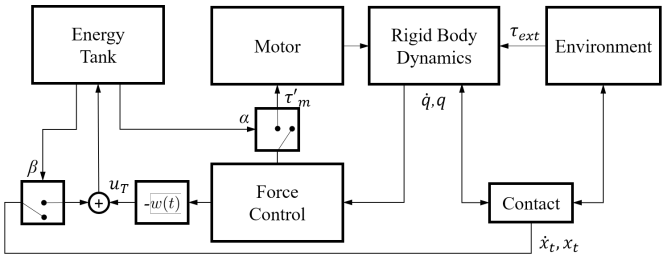

Fig. 2: Block diagram of the proposed force controller via energy-tanks.

where $\dot{x}_t$ is the time derivative of the tank state, $\tilde{x}$ represents the error between desired and actual states. The term $w(t)$ represents the tank control input, and lastly β is defined as:

$$\beta = \begin{cases} 1 & \text{if } \; T \leq T_{upper} \\ 0 & \text{otherwise} \end{cases} \tag{5}$$

β is a design parameter that enables the storage of dissipated energy as long as the total tank energy is below its upper bound T_{upper}. Differently, if the tank energy is greater than T_{upper}, β becomes zero and the tank is disabled. This condition allows to prevent excessive storage. The product $(\dot{\tilde{x}}^T D_d \, \dot{\tilde{x}})$ represents the power dissipated. The tank control input $w(t)$ is defined as:

$$w(F_{ext}, t) = \frac{\alpha}{x_t}\Big(k_p(F_{ext} - F_d) - k_i \int_0^t \big(F_{ext}(t) - F_d(t)\big)\Big) \tag{6}$$

Therefore we are now able to write the extended motor dynamics as:

$$\tau'_m = J^T(\mathbf{q})\frac{\alpha}{x_t}\Big[k_p(F_{ext} - F_{des}) + k_i \int_0^t (F_{ext} - F_{des})\Big] \tag{7}$$

where α is defined as:

$$\alpha = \begin{cases} 1 & \text{if } \; T \geq T_{lower} \\ 0 & \text{otherwise} \end{cases} \tag{8}$$

where $T_{lower} > 0$ represents the lower bound below which the energy cannot be extracted by the tank, leading to $\alpha = 0$ and preventing singularities to occur. The proposed approach is illustrated in the block diagram of Fig. 2.

III. MANIPULATION SYSTEM

A. Design Considerations

A recurrent approach found in the state-of-the-art of aerial manipulation is to make use of multiple-DoFs manipulators and serial arms to carry out low-dexterity manipulation tasks airborne. Despite the added benefit of having additional *n* DoFs on the aerial system, several drawbacks come with it. First to mention is the increased weight that *n* additional actuators add the to the aerial platform, posing a tight constraint to battery life and manoeuvrability [21]. Another disadvantage typical of high-DoFs manipulators is the higher kinematics and control complexity, which often require higher processing power and longer computation time to be solved. In general, several aerial applications may require limited manipulation capabilities, such as force-driven tasks for non-destructive-testing, contact-based inspection or simply tactile sensing for motion planning purposes. These types of operations can be achieved with a simple probe oriented towards the contact surface providing the aerial system with a minimal, weight-efficient solution to the problem.

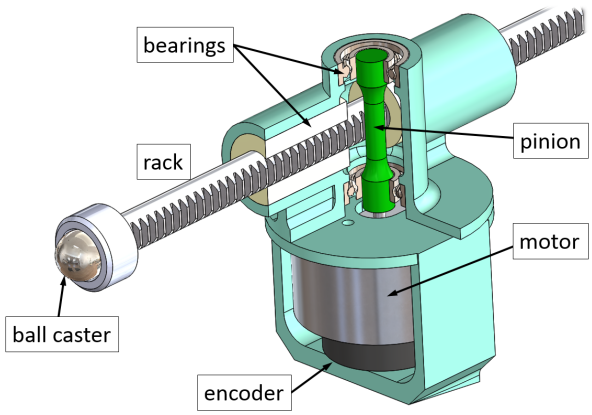

Fig. 3: Computer-Aided-Drawing of the manipulator's transmission mechanism enclosed in a cross-shaped casing. For clarity reasons, the distance sensor and other electronic components are not displayed in this figure.

B. Manipulator Design

The proposed design consists of a single-DoF manipulator embodied by a prismatic joint. The actuator on-board converts rotational motion into linear by means of a rack and pinion transmission, allowing the end-effector to slide inside the joint casing. The pinion is attached on the motor shaft directly, without any gear reduction in place. The motor chosen for this design is a DC brushless, selected for its high torque to weight ratio, increased efficiency and reliability when compared to other types of motors. The rack and pinion components are manufactured in aluminium to ensure an accurate transmission and reduce the mass. Two linear bearings guarantee adherence of the rack's teeth in the linear coupling. Similarly, two ball bearings hold the pinion in place perpendicularly to the rack, and release the motor from any radial tension that might be generated during interaction. The manipulator's design is displayed in Fig. 3.

The end-effector is chosen to be a metal ball caster, mounted at the tip of the rack (see Fig. 3). The ball caster is selected as it minimises friction and allows for smooth contouring even on indentations that might be present on the target surface. The ball caster is also ideal as it reduces the contact surface to a single point, therefore zeroing the moments of the external wrench τ_{ext} leading to pure force exchange F_{ext}.

Lastly, the manipulator design incorporates 2 sensors: an inductive encoder on the brushless motor which measures the relative position of the end-effector; and a distance sensor mounted at the front of the aircraft to measure the relative position of the vehicle with respect to the target ahead.

IV. EXPERIMENTS

In this section, the flight experiments of the proposed system are presented and discussed. The objective is to

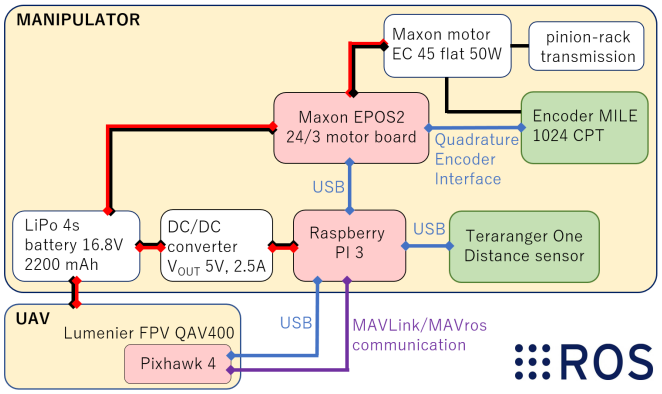

Fig. 4: Experimental setup of the aerial manipulator during flight experiments: components and connections. All the controller boards of this setup are displayed in red boxes, while green boxes represent sensing of the aerial manipulator.

demonstrate the ability of the aerial system to apply a shear force for a prolonged period of time over a surface and minimize contact loss with the target.

A. Experimental Setup

The platform used for flight experiments is the quadcopter Lumenier QAV400® (1.1kg) with flight controller Pixhawk 4®. The manipulator on-board computer is a Raspberry PI 3 (1.4 GHz 64-bit quad-core ARM Cortex-A53 processor) with Wi-Fi capabilities. The slider joint is actuated by a brushless Maxon® motor EC 45 flat (50 Watt, 780 mNm stall torque, with Hall sensor and digital encoder). The motor controller board is the high-performance Maxon® EPOS2 24/3 digital board, sampling at a rate of 10 kHz and allowing real-time control of the end-effector. The distance sensor TeraRanger® One is mounted at the front of the aircraft measuring the UAV's relative position with respect to the obstacle in front. The sensor sampling rate is 1 kHz. The manipulator total mass is 500 g, and the aircraft all-up-weight is 1.85 kg. The software implementation is in ROS. Ground-truth measurements of the UAV states in-flight are acquired by a VICON motion capture system. Figure 4 illustrates the experimental setup.

B. Results

The outline of the experiments is as follow: the UAV approaches the target surface and once the vehicle's angular states and relative position from the target are within a certain threshold, the manipulator autonomously initiates the task. The UAV states measured by the flight controller are communicated to the manipulator's on-board computer via a MAVLink/MAVros bridge, whilst the on-board distance sensor provides the range information. After the end-effector is extended and contact is established with the surface, the UAV flies sideways while facing the target and the manipulator exerts a constant force over the surface. As the obstacle becomes out of range, the manipulation task terminates and the end-effector slowly retracts.

The main challenge faced in these airborne tests is the ability to keep continuous contact with the target for a prolonged period of time whilst the vehicle is moving. To do

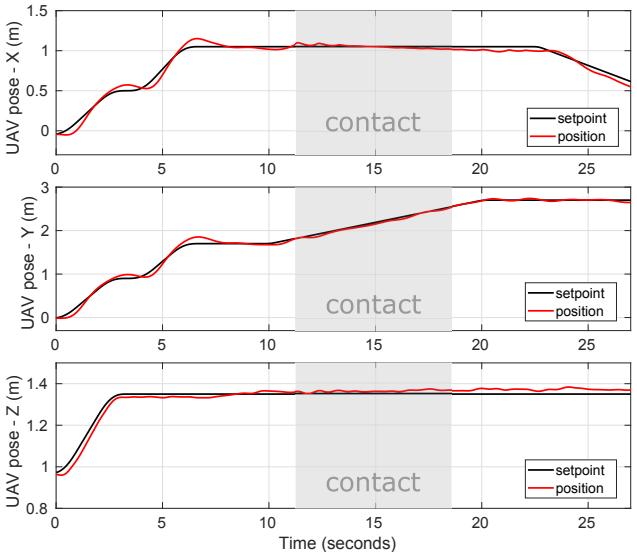

(a) UAV pose along x-y-z axes.

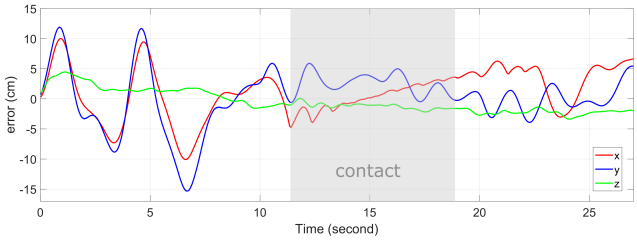

(b) Positioning error of the UAV along x-y-z axes.

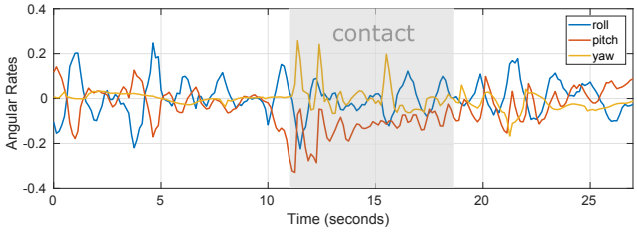

(c) UAV angular rates.

Fig. 5: Data captured during a single flight experiment illustrating the UAV positioning error and angular states while exerting a 5 N shear force over a 2D surface.

so, the manipulator's controller has to overcome any drifting that might be present in the vehicle, caused by for example turbulence in the proximity of the obstacle, or an error in the UAV's positioning estimate. Figure 5(a) shows the UAV x-y-z coordinates during the task compared to the setpoint. We can see that the UAV is able to keep a relatively low error in pose as it executes the waypoint mission.

The positioning error along x-y-z axes is illustrated in 5(b). It can be noticed that the x-y values reach 15 cm as the vehicle moves in between waypoints, while they remain below 5 cm during the interaction task. This is because the UAV velocity outside the task domain was set as $v = 0.5\ m/s$ as opposed to $v = 0.1\ m/s$ during contact, causing additional drifting. Looking at the error in x during contact we can notice how it increases in a linear trend. This error is induced by the manipulator extending further in the x-direction, pushing the vehicle's centre-of-gravity

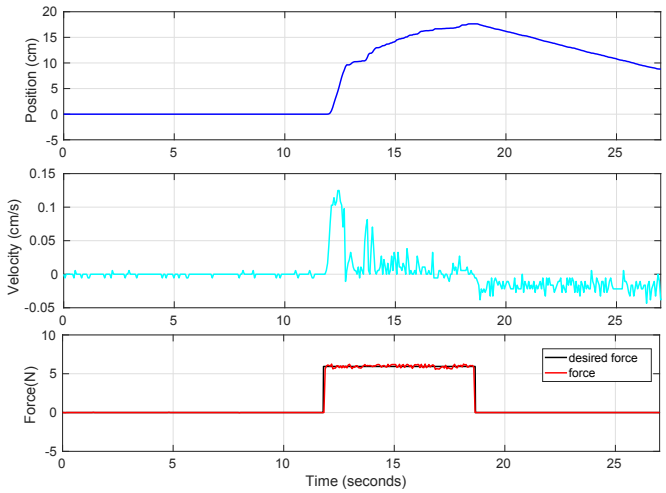

Fig. 6: From top to bottom: manipulator position and velocity states and force exerted at the end-effector.

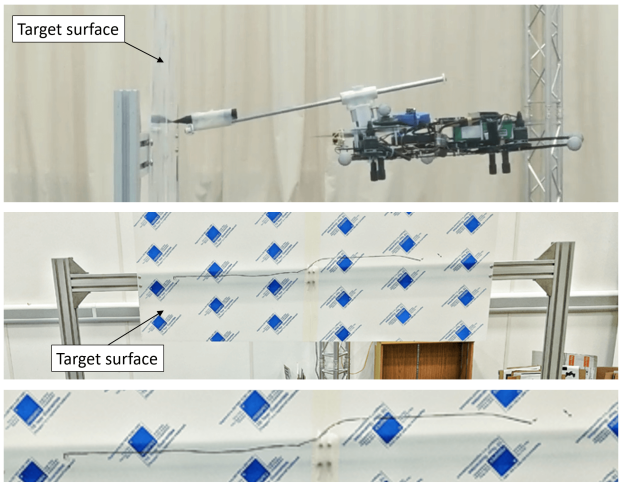

Fig. 7: Continuous contact between the aerial manipulator and the target surface is demonstrated with the use of a pen marker, which allows the aerial system to draw a continuous line over a length of 1.25 metres.

backwards with respect to the wall. The error along z is fairly low throughout the entire experiment, i.e. on average less than 2 cm. Figure 5(c) shows the vehicle angular rates. It can be seen that both the *pitch* and *yaw* rate have peak oscillations as the the end-effector makes contact with the wall. From t = 12.5 s until the end of the task the angular rates remain below 0.2, showing that disturbances sensed by the vehicle are low throughout the interaction, despite the fact that the manipulator is applying a force over 5 N on the target (see Fig. 6, *bottom*). Overall Fig. 6 displays the end-effector position and velocity states, along with the force generated at the end-effector.

Figure 7 displays a side view of the aerial manipulator during experiments. The ball caster tip has been replaced by a marker pen to give the reader a better visualisation on the performance accuracy, as the manipulator draws a line on the target surface. The line is drawn on the whole length of the panel (approximately 1.25 m) and without interruptions.

Looking at figures 7 and 5(b) we can appreciate that the error on the z axis (the axis pointing to the ceiling) remains below 1 cm during the interaction task, resulting in a straight line on the target surface. A small drop in height is visible in the middle section of the target surface due to the presence of fixtures on the mounting structure (see Fig. 7).

Overall, a total number of 15 experiments has been conducted. A successful outcome was assigned to those experiments where the end-effector kept in continuous contact throughout the entire length. Overall, a success rate of 86% was reached.

V. CONCLUSIONS

Within this paper, we have presented the first example of energy tank-based force control applied by an unmanned aerial vehicle for 2D contour following tasks. This approach successfully allows to apply shear constant forces to unknown surfaces for prolonged periods of time, proving suitable to aid tactile-driven tasks. With these initial results, success rates of over 85% were achieved, offering the potential for tracing out more complex and highly variable 3D surfaces in the future.

Although in the initial stages of development, energy tank-based methods can offer significant benefit to aerial manipulators, providing a reliable and robust approach towards interaction control. Future work will build on this approach by combining variable-compliance manipulation and visual sensing to trace around more complex shapes.

REFERENCES

[1] A. Suarez, G. Heredia, and A. Ollero, "Lightweight compliant arm for aerial manipulation," in *Intelligent Robots and Systems (IROS), 2015 IEEE/RSJ International Conference on*, pp. 1627–1632, IEEE, 2015.

[2] A. Suarez, G. Heredia, and A. Ollero, "Lightweight compliant arm with compliant finger for aerial manipulation and inspection," in *Intelligent Robots and Systems (IROS), 2016 IEEE/RSJ International Conference on*, pp. 4449–4454, IEEE, 2016.

[3] T. Bartelds, A. Capra, S. Hamaza, S. Stramigioli, and M. Fumagalli, "Compliant aerial manipulators: Toward a new generation of aerial robotic workers," *IEEE Robotics and Automation Letters*, pp. 477–483, Jan 2016.

[4] M. Bisgaard, A. la Cour-Harbo, and J. D. Bendtsen, "Adaptive control system for autonomous helicopter slung load operations," *Control Engineering Practice*, vol. 18, no. 7, pp. 800–811, 2010.

[5] F. Forte, R. Naldi, A. Macchelli, and L. Marconi, "Impedance control of an aerial manipulator," in *American Control Conference (ACC), 2012*, pp. 3839–3844, IEEE, 2012.

[6] G. Giglio and F. Pierri, "Selective compliance control for an unmanned aerial vehicle with a robotic arm," in *Control and Automation (MED), 2014 22nd Mediterranean Conference of*, pp. 1190–1195, IEEE, 2014.

[7] E. Cataldi, G. Muscio, M. A. Trujillo, Y. Rodríguez, F. Pierri, G. Antonelli, F. Caccavale, A. Viguria, S. Chiaverini, and A. Ollero, "Impedance control of an aerial-manipulator: Preliminary results," in *Intelligent Robots and Systems (IROS), 2016 IEEE/RSJ International Conference on*, pp. 3848–3853, IEEE, 2016.

[8] S. Hamaza, I. Georgilas, and T. Richardson, "Towards an adaptive-compliance aerial manipulator for contact-based interaction," in *2018 IEEE/RSJ International Conference on Intelligent Robots and Systems (IROS)*, p. in press, IEEE, 2018.

[9] S. Hamaza, I. Georgilas, and T. Richardson, "An adaptive-compliance manipulator for contact-based aerial applications," in *2018 IEEE/ASME International Conference on Advanced Intelligent Mechatronics (AIM)*, pp. 730–735, IEEE, 2018.

[10] J. De Schutter, T. De Laet, J. Rutgeerts, W. Decré, R. Smits, E. Aertbeliën, K. Claes, and H. Bruyninckx, "Constraint-based task specification and estimation for sensor-based robot systems in the

presence of geometric uncertainty," *The International Journal of Robotics Research*, vol. 26, no. 5, pp. 433–455, 2007.

[11] G. Borghesan and J. De Schutter, "Constraint-based specification of hybrid position-impedance-force tasks," in *Robotics and Automation (ICRA), 2014 IEEE International Conference on*, pp. 2290–2296, IEEE, 2014.

[12] M. H. Raibert and J. J. Craig, "Hybrid position/force control of manipulators," *Journal of Dynamic Systems, Measurement, and Control*, vol. 103, no. 2, pp. 126–133, 1981.

[13] C. Schindlbeck and S. Haddadin, "Unified passivity-based cartesian force/impedance control for rigid and flexible joint robots via task-energy tanks," in *2015 IEEE international conference on robotics and automation (ICRA)*, pp. 440–447, IEEE, 2015.

[14] A. Y. Mersha, S. Stramigioli, and R. Carloni, "Variable impedance control for aerial interaction," in *Intelligent Robots and Systems (IROS 2014), 2014 IEEE/RSJ International Conference on*, pp. 3435–3440, IEEE, 2014.

[15] H. W. Wopereis, J. Hoekstra, T. Post, G. A. Folkertsma, S. Stramigioli, and M. Fumagalli, "Application of substantial and sustained force to vertical surfaces using a quadrotor," in *2017 IEEE International Conference on Robotics and Automation (ICRA)*, pp. 2704–2709, IEEE, 2017.

[16] F. Ferraguti, C. Secchi, and C. Fantuzzi, "A tank-based approach to impedance control with variable stiffness," in *Robotics and Automation (ICRA), 2013 IEEE International Conference on*, pp. 4948–4953, IEEE, 2013.

[17] F. Ferraguti, N. Preda, A. Manurung, M. Bonfe, O. Lambercy, R. Gassert, R. Muradore, P. Fiorini, and C. Secchi, "An energy tank-based interactive control architecture for autonomous and teleoperated robotic surgery," *IEEE Transactions on Robotics*, vol. 31, no. 5, pp. 1073–1088, 2015.

[18] M. Franken, S. Stramigioli, S. Misra, C. Secchi, and A. Macchelli, "Bilateral telemanipulation with time delays: A two-layer approach combining passivity and transparency," *IEEE transactions on robotics*, vol. 27, no. 4, pp. 741–756, 2011.

[19] A. Franchi, C. Secchi, H. I. Son, H. H. Bulthoff, and P. R. Giordano, "Bilateral teleoperation of groups of mobile robots with time-varying topology," *IEEE Transactions on Robotics*, vol. 28, no. 5, pp. 1019–1033, 2012.

[20] C. Secchi, A. Franchi, H. H. Bülthoff, and P. R. Giordano, "Bilateral teleoperation of a group of uavs with communication delays and switching topology," in *Robotics and Automation (ICRA), 2012 IEEE International Conference on*, pp. 4307–4314, IEEE, 2012.

[21] F. Huber, K. Kondak, K. Krieger, D. Sommer, M. Schwarzbach, M. Laiacker, I. Kossyk, S. Parusel, S. Haddadin, and A. Albu-Schaffer, "First analysis and experiments in aerial manipulation using fully actuated redundant robot arm," in *Intelligent Robots and Systems (IROS), 2013 IEEE/RSJ International Conference on*, pp. 3452–3457, IEEE, 2013.